
Progressive Gradient Flow for Robust N:M Sparsity Training in Transformers

Abhimanyu Rajeshkumar Bambhaniya^{*1} Amir Yazdanbakhsh^{*2} Suvinay Subramanian³ Sheng-Chun Kao³
 Shivani Agrawal³ Utku Evci² Tushar Krishna¹

Abstract

N:M Structured sparsity has garnered significant interest as a result of relatively modest overhead and improved efficiency. Additionally, this form of sparsity holds considerable appeal for reducing the memory footprint owing to their modest representation overhead. There have been efforts to develop training recipes for N:M structured sparsity, they primarily focus on low-sparsity regions ($\sim 50\%$). Nonetheless, performance of models trained using these approaches tends to decline when confronted with high-sparsity regions ($>80\%$). In this work, we study the effectiveness of existing sparse training recipes at *high-sparsity regions* and argue that these methods fail to sustain the model quality on par with low-sparsity regions. We demonstrate that the significant factor contributing to this disparity is the presence of elevated levels of induced noise in the gradient magnitudes. To mitigate this undesirable effect, we employ decay mechanisms to progressively restrict the flow of gradients towards pruned elements. Our approach improves the model quality by up to 2% and 5% in vision and language models at high sparsity regime, respectively. We also evaluate the trade-off between model accuracy and training compute cost in terms of FLOPs. At iso-training FLOPs, our method yields better performance compared to conventional sparse training recipes, exhibiting an accuracy improvement of up to 2%. The source code is available at GitHub.

1. Introduction

A prevailing tendency in state-of-the-art DNN models is the rapid increase in their model (Raffel et al., 2019; Zhang et al., 2022a; OpenAI, 2023; Touvron et al., 2023; Anil et al.,

^{*}Equal contribution ¹Georgia Institute of Technology ²Google DeepMind ³Google. Correspondence to: Amir Yazdanbakhsh <ayazdan@google.com>.

2023). To address the deployment challenges of these models, a large body of research proposes quantization (Shen et al., 2020; Kim et al., 2021; Zafrir et al., 2019; Zhang et al., 2020), sparsification (Evci et al., 2019; Han et al., 2015a; Guo et al., 2016; He et al., 2017; Molchanov et al., 2016; Yao et al., 2019; Zhu & Gupta, 2017), and distillation (Gou et al., 2021). This paper centers its attention on *sparsification/pruning* offering the following benefits: (a) improved performance (Zhou et al., 2021), (b) reduce memory usage (Qin et al., 2021), and (c) higher energy efficiency (Akhlaghi et al., 2018; Pan et al., 2023).

While appealing, sparsification predominantly revolves around the inherent trade-offs between the quality of the model and compression ratio¹. For example, some studies (Guo et al., 2016; Han et al., 2015b) have demonstrated promising results in achieving unstructured sparsity levels of around 90%-95% in image classification models, while maintaining the quality of dense models. Similarly, the noticeable achievements of transformer-based models, primarily driven by their exponential growth in model size (Wei et al., 2022), have stimulated interest (Child et al., 2019; Beltagy et al., 2020; Roy et al., 2021; Kitaev et al., 2020) in exploring sparsification recipes for such models with high sparsity ratio. This serves as a significant incentive for the sparsification of attention-based models, as it enables the pruning of a substantial number of model parameters ($>70\%$) (Tay et al., 2022; Jaszczur et al., 2021). Despite its inherent ability to trim the memory footprint of large models, the realization of unstructured sparsity in hardware poses nontrivial challenges for acceleration. The sparsity-induced models frequently exhibit comparable or inferior performance to their dense counterparts because of the additional intricacies involved in compression/decompression of model parameters (Nvidia, 2021a; Ma et al., 2021; Renda et al., 2020; Lin et al., 2021; Gamboa et al., 2020; Zhu et al., 2019).

As such, structured sparsity has gained significant popularity because of its hardware-friendly characteristics. (Yao et al., 2019; Kang, 2019; Parashar et al., 2017; Liu et al.,

¹We designate algorithmic-wise factors such as accuracy, recall, and precision as *model quality*. and denote model runtime/latency as *model performance*.

2022b; Jeong et al., 2023; Bambhaniya et al., 2023; Qin et al., 2022) found that employing fine-grained N:M structured sparsity, has the potential to mitigate the degradation in quality. Moreover, the debut of 2:4 structured-sparse tensor core in GPU Ampere architecture (Nvidia, 2021a) has generated additional enthusiasm in developing efficient N:M training recipes. Although recent methods (Pool & Yu, 2021; Mishra et al., 2021; Nvidia, 2021b; Zhou et al., 2021; Lu et al., 2023; Frantar & Alistarh, 2023) demonstrate acceptable quality, their main focus lies in addressing sparsity levels up to 2:8. These methods, however, less effective when dealing with high sparsity regimes such as 1:16, 1:32, and higher. Through our studies, we identify that elevated levels of induced noise in the gradient magnitudes constitute a notable contributing factor to such quality degradation. This phenomenon can be primarily attributed to either the absence (Johnson & Zhang, 2013; Wang et al., 2013) or perturbation of gradient flow of existing sparse training recipes. Building on the insights our experiments, we introduce alternative training recipes that demonstrate substantial improvements in model quality, particularly at high sparsity regime. We made the following contributions:

- **The impact of gradient perturbations becomes increasingly evident at elevated levels of sparsity, leading to a deterioration in the quality of the model.** We present empirical evidence that SR-STE, a state-of-the-art N:M structured training recipe (Zhou et al., 2021), is less effective at high sparsity regions, $> 75\%$. We attribute this to the nontrivial perturbation of gradient magnitudes. This perturbation during the initial stages of training² adversely amplifies the variance of gradients, resulting in a diminished model quality.
- **Gradient flow is all you need.** In order to alleviate the adverse effects of noisy gradients, we introduce a class of decaying-based sparse training recipes tailored for N:M structured sparsity. The fundamental principle underlying these methods involves progressively limiting the flow of gradients for *pruned weights*, while allowing the gradients to freely flow at the early stages of training. Our results demonstrate that the decaying-based methods consistently outperform SR-STE by up to 2%-5% in terms of model quality, while pruning $\sim 97\%$ of parameters.
- **Decaying-based sparse training recipes require less training FLOPs.** To better understand the computational overhead of the proposed sparse training recipes, we present the trade-off between model accuracy and training compute cost in term of FLOPs. The results show that at iso-quality, our method requires $> 30\%$ fewer training FLOPs compared to SR-STE.

²Recent studies for dense models (Lu et al., 2023; Johnson & Zhang, 2013) have shown that the early stage of training (critical region) is imperative in the quality of training recipes.

2. Background and Related Works

This work focuses on weight sparsity, which poses a significant challenge in serving transformer-based models.

2.1. Computation Flow of Sparse Training Recipes

Figure 1 summarizes the computation flows of various training recipes for the sparsification of model parameters. A sparsification recipe broadly entails 1) pruning criteria, 2) pruning schedule, and 3) sparsity pattern.

(1) Pruning criteria. The pruning criteria refers to the set of criteria used to determine the specific elements within the weight tensor that should be pruned. Magnitude pruning, which selects the pruning elements based on their absolute values, is one of the most widely used criteria for sparsification (Renda et al., 2020; Guo et al., 2016; Lee et al., 2019; Frankle & Carbin, 2019; Gale et al., 2019; Zhu & Gupta, 2017; Han et al., 2015a; Liu et al., 2018). Recent work employs other criteria such as gradient (Yeom et al., 2021; Evci et al., 2020), Hessian (LeCun et al., 1989), connection sensitivity (Lee et al., 2019), and importance estimation (Molchanov et al., 2019). In this paper, we use magnitude pruning, following SR-STE (Zhou et al., 2021) the state-of-the-art structured N:M training recipe.

(2) Pruning schedule. We classify the pruning schedules into the following broad categories:

- **Fine-tuning with one-shot pruning**→ This approach (Mishra et al., 2021; Pool & Yu, 2021; Frankle & Carbin, 2019; Lee et al., 2019) involves training a dense model, followed by on-shot weight pruning. Subsequently the pruned model is fine-tuned to regain the lost quality.
- **Fine-tuning with iterative pruning**→ This method (Evci et al., 2019; Han et al., 2015a; Guo et al., 2016; He et al., 2017; Molchanov et al., 2016; Yao et al., 2019; Zhu & Gupta, 2017; Gamboa et al., 2020; Narang et al., 2017a;b; Elsen et al., 2020; Evci et al., 2020) trains a dense model followed by iterative cycles of pruning and re-training, which shows a greater capacity to regain lost quality.
- **From-scratch with learned pruning pattern**→ This pruning recipe (Frankle et al., 2020; Evci et al., 2019) establishes the sparsity pattern based on pretrained dense model and subsequently trains a sparse model from scratch.
- **From-scratch while learning sparsity pattern**→ This approach (Wortsman et al., 2019; Dettmers & Zettlemoyer, 2019; Gale et al., 2019; Kusupati et al., 2020; Evci et al., 2020; Bellec et al., 2018; Mocanu et al., 2018) trains a sparse model from scratch while concurrently learning the sparsity mask.

(3) Sparsity pattern. We broadly categorize sparsity patterns into following groups:

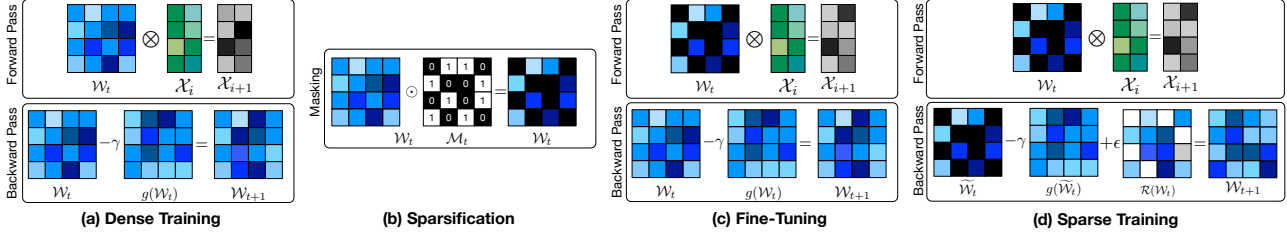


Figure 1. The computation flow of (a) dense training, (b) sparsification, (c) fine-tuning, and (d) sparse training (e.g. SR-STE). \tilde{W} represents a pruned matrix that is computed by element-wise multiplication (\odot) of W and its sparsification mask (\mathcal{M}). Sparse training recipes, such as SR-STE, introduce a “sparse refining” regularizer (\mathcal{R}) to adjust the gradient terms for pruned elements.

- **Unstructured Sparsity** refers to the process of pruning a model without imposing any constraints on the sparsity pattern (Renda et al., 2020; Guo et al., 2016; Lee et al., 2019; Frankle & Carbin, 2019; Gale et al., 2019). This sparsity pattern is known to be able to prune the model size to an order of magnitude smaller while retaining a similar model quality as its dense counterpart at the cost of increased runtime overhead.
- **Coarse-grained Structured Sparsity** enforces coarse-grained sparsity patterns, including techniques like filter/channel pruning (Li et al., 2016; Wen et al., 2016; He et al., 2017) and block-wise pruning (Wen et al., 2016; Ma et al., 2021; Narang et al., 2017b; Gray et al., 2017). By skipping the entire computation of a tensor, this sparsity pattern often yields speedup in natively-dense accelerators such as GPUs and TPUs. Nevertheless, this trade-off often results in a reduction in model quality.
- **Fine-grained Structured N:M Sparsity** prunes (M-N) out of M consecutive elements. Several preliminary studies rely on special threading and grouping techniques (Yao et al., 2019) or specialized sparse accelerators (Kang, 2019) to exploit this fine-grained sparsity pattern. With the inclusion of 2:4 GEMM support in GPU Ampere architecture (Nvidia, 2021a), recent work starts to investigate effective training recipes for N:M sparsity patterns to harness the existing accelerators (Pool & Yu, 2021; Mishra et al., 2021; Nvidia, 2021b; Zhou et al., 2021).

Other related work. Other work has also investigated N:M structured sparsity in attention-based models. SR-STE (Zhou et al., 2021) proposes a training recipe with fine-grained N:M structured sparsity from scratch. Figure 2(a) demonstrates the weight update scheme for the forward and backward pass of SR-STE. Nvidia ASP (Nvidia, 2021b) focuses on low sparsity (2:4) and employs channel permutations to maximize the accuracy of N:M sparse networks. However, this approach becomes slow for higher sparsification levels because of the lack of hardware support. SparseGPT (Frantar & Alistarh, 2023) introduces a post-training sparsification recipe tailored for GPT-family models. SparseGPT shows on-par model quality with up to 50%

weight pruning under unstructured and N:M structured sparsity. Finally, selective weight decay (SWD) (Tessier et al., 2022) is a pruning method based on Lagrangian smoothing, which penalizes weights that are selected for pruning. However, SWD neither explores attention models nor provides training recipes for N:M structured sparsity.

3. Decaying-based Sparse Training Recipes

This section covers the class of decaying-based training recipes for fine-grained N:M sparsity. The main premise of these recipes is to allow the gradient to flow through weight tensors in a controlled way to prevent induced noise in the gradients. We broadly classify the proposed decaying-based training recipes into: (a) “**M**ask **D**ecay **G**radient **F**low” (MDGF) and (b) “**S**tructure **D**ecay **G**radient **F**low” (SDGF), each with sub-variants which we discuss in details below. In contrast to (Zhou et al., 2021), we intentionally refrain from modifying the gradient update rules in either of these categories. Instead, we use different update rules for sparsity pattern or sparsity mask tensor, facilitating unimpeded gradient flow during the entire sparse training process.

Implementation. In order to implement these methods, we employ the process of pruning dense weight tensors (W_t) to generate sparse weight tensors (\tilde{W}_t), adhering to the following rule during the forward pass:

$$\begin{aligned} \tilde{W} &= \mathcal{F}(W, N, M, \Phi, \beta, j) \\ &= W \odot [\Phi(W, N, M, j) + \mathcal{D}(j)(1 - \Phi(W, N, M, j))] \end{aligned}$$

Here \odot represents the Hadamard product. $\Phi(\cdot)$ and $\mathcal{D}(\cdot)$ calculate a decaying-based binary mask and decay mask factor, respectively. Each function’s implementations establish distinct decaying-based training recipes. $\Phi(\cdot)$ calculates a binary mask that matches the dimensions of the input weight tensor (W). The location of 0s and 1s in the binary mask refers to pruned and unpruned weights, respectively. In fine-grained N:M structured sparsity with magnitude pruning, $\Phi(\cdot)$ assigns a value of 1 to the N weight tensor elements with the highest absolute magnitude within a contiguous block of M elements. Simultaneously, it enforces all the

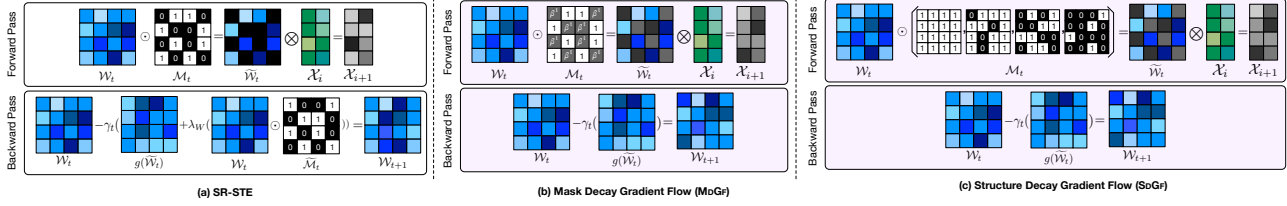


Figure 2. An overview of different sparse training recipes (a) SR-STE (Zhou et al., 2021), (b, c) proposed decaying mechanisms in this work. (b) indicates decaying binary mask values for pruned weights (MDGF), whereas (c) gradually change the N:M sparsity patterns at different intervals (SDGF).

other elements with the block to be set to 0. In addition, $\mathcal{D}(\cdot)$ calculates the decaying factor for binary mask according to the target decaying-based training recipe.

1 Mask Decay Gradient Flow (MDGF). In the first training recipe Figure 2 (b), we propose the use of a diminishing value ranging from 1 to 0, as opposed to the commonly-used binary pruning mask (e.g., “0” \rightarrow pruned and “1” \rightarrow dense). Note that for the mask-decay training recipes the function $\Phi(\cdot)$ produces a mask tensor either with all ones (dense training) or with a sparsity pattern following target N:M fine-grained structured sparsity. In the initial epochs, we use a mask comprising solely of ones and assign a constant value of 1 to $\mathcal{D}(\cdot)$, i.e., dense training.

Upon starting sparse training phase, $\mathcal{D}(\cdot)$ produces gradually diminishing floating-point values between 1 and 0. The output of function $\mathcal{D}(\cdot)$ depends on current decaying interval. Using a diminishing decaying factor enables gradient flow for both pruned and unpruned weights. This is in contrast to prior work in which $\mathcal{D}(\cdot)$ is null which may cause instability in the training process. We propose two alternative implementations for $\mathcal{D}(\cdot)$ as follows:

- MDGF-Linear uses $\mathcal{D}(j) = \max(1 - K_\tau \times j, 0)$ that reduces the decay mask values linearly with respect to training steps.
- MDGF-Exponential, as its name implies, we use $\mathcal{D}(j) = e^{-K_\eta \times j}$, indicating an exponential decrease in the mask decay value relative to the ongoing training step.

The value of $K_{\tau/\eta}$ determines the rate of decay. To ensure a binary mask value for the target N:M sparsity pattern, after sufficient decaying intervals, $\mathcal{D}(\cdot)$ approaches zero. After reaching the target N:M sparsity pattern, we proceed with few additional training epochs to restore the model accuracy. We postulate that using non-binary pruning mask values facilitates the smooth propagation of gradients in pruned weights, resulting in more stable sparse training.

2 Structure Decay Gradient Flow (SDGF). SDGF decays the structure of the pruning mask, e.g. gradually altering the sparsity level, e.g. $\frac{3}{4} \mapsto \dots \mapsto \frac{1}{4}$. In contrast to MDGF, this method strictly confines the pruning mask values to

either 1 or 0, e.g. $\mathcal{D}(\cdot) = 0$. We propose two alternative implementations of $\Phi(\cdot)$, (a) *Stepwise* and (b) *Geometric*.

The SDGF-*Stepwise* starts by inducing M-1:M structured sparsity. Subsequently, it gradually increase the level of sparsity following $\frac{M}{2^d} : M$ formulation in which d denotes the index of the decaying interval, until $\frac{M}{2^d} = N$. For example, to retain a target sparsity level of 1:8, the method applies the following sparsity patterns at different decaying interval $\frac{7}{8} \mapsto \frac{4}{8} \mapsto \frac{2}{8} \mapsto \frac{1}{8}$.

The core idea of SDGF-*Geometric* is to maintain a constant ratio of $\frac{N}{M}$ throughout successive decay intervals by adjusting the values of N and M in proportion to each other. In all experiments, we configure $\Phi(\cdot)$ to be $\frac{k \times M}{2^d} : \frac{k \times N}{2^d}$. The value of k is set to 16, unless specifies otherwise. We empirically find that $k > 16$ offers negligible improvements in terms of model quality. For example, for a target sparsity of 1:8, we induce the following sparsity patterns at each decaying interval, $\frac{16}{128} \mapsto \frac{8}{64} \mapsto \frac{4}{32} \mapsto \frac{2}{16} \mapsto \frac{1}{8}$. For both recipes, we evenly partition the total sparsification epochs throughout the decaying intervals. Fundamentally, this approach follows a hypothesis akin to MDGF. Enabling the flow of gradients of pruned weights throughout the model potentially leads to higher model accuracy.

4. Impact of Gradient Flow in Sparsification

To gain better understanding of the advantages of proposed decay methods, we conducted an empirical analysis to compare the gradient values of MDGF-Exponential and SR-STE (Zhou et al., 2021). We created a compact version of ViT with three encoder layers, each with three attention heads, and an embedding size of 192. We trained this model on CIFAR-10 (Krizhevsky et al., 2009) for 200 epochs with batch size 64 with AdamW optimizer. To understand the impact of sparsification, we collect and analyze two different metrics, namely *second moment* and *gradient variance*. These values are an indication of how effective the gradient estimations are for training (Tang et al., 2021; Lu et al., 2022; Li et al., 2022).

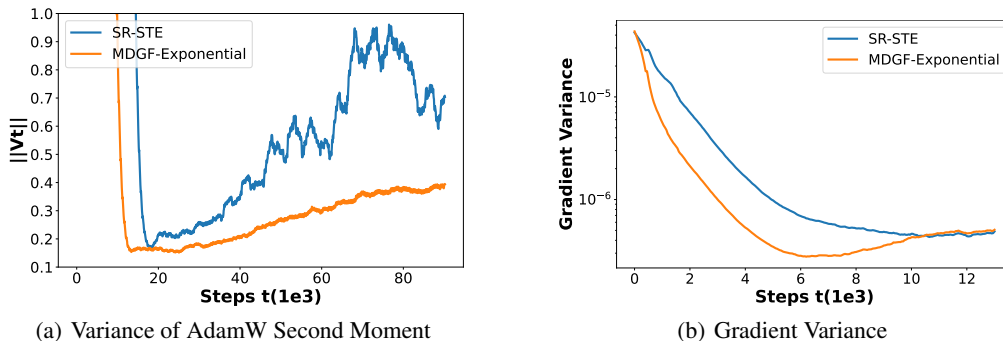


Figure 3. Trends for different indicators of gradient values during training. Data from ViT-tiny trained on CIFAR-10 with 1:16 sparsity pattern. (a) and (b) show the running average of the variance of AdamW second moment and gradient variance, respectively.

4.1. Analysis of Second Moment Estimates

Figure 3(a) shows the variance of the second moment term (exponential moving average of squared gradient values) for Feed-Forward (FF) layers in the model. We observe that in MDGF, the variance steadily decreases in magnitude, whereas in SR-STE, the variance stays at the relatively high level even at the later stages of training. Prior study (Tang et al., 2021; Lu et al., 2022; Li et al., 2022) correlate lower variance of the second moment with faster convergence rate during training and better model accuracy. This suggests that the gradient noise induced by SR-STE have negative impact on the convergence of the model and model accuracy.

4.2. Analysis of Gradient Noise

Figure 3(b) shows the variance of absolute back-propagation gradients. These values can be interpreted as the amount of noise in the gradient estimates. Similar to the previous study, we collect the gradients of Feed-Forward(FF) layer in tiny-ViT. We observe that in MDGF, the variance of gradients decreases quickly, whereas in SR-STE, the variance of gradients has a lower slope (e.g. taking a larger number of steps). When the variance of the gradient is higher, the optimizer spends time bouncing around, leading to slower convergence and lower performance (Johnson & Zhang, 2013; Wang et al., 2013). The variance for MDGF-Exponential comes down rather quickly thus the gradients are less noisy compared to SR-STE. This would result in higher accuracy for MDGF-Exponential. When observing the final validation accuracy of the two runs, we confirm our intuitive conclusions as the SR-STE accuracy is lower compared to MDGF-Exponential accuracy.

5. Experiment

In this section, we evaluate the effectiveness of various training recipes for N:M fine-grained structured sparsity in a range of attention-based models and tasks, such as image classification, language translation and understanding.

Motivated by the relatively substantial contribution of FF layers (Table 1) in total FLOPs ($\sim 64\%$) and parameter count ($\sim 66.6\%$), we center our experiments around sparsification of these layers within the encoder and decoder blocks. In addition, we conduct experiments on the pruning of projection layers ($\mathcal{Q}/\mathcal{K}/\mathcal{V}$) for a variant of ViT-Base (Dosovitskiy et al., 2021), a variant of SwinV2-Base (Liu et al., 2022a), and T5X-Base (Raffel et al., 2019). For ViT-Base, we use fixed-size patches (resolution 16×16) on images with resolution 224. In SwinV2-Base, we employ window sizes of 8×8 on images with resolution 256. For image classification tasks, we branched (commit: 1304589) our implementation from PyTorch Image Models (Wightman, 2019) and use NVIDIA A100 GPUs for training on ImageNet-1K dataset (Deng et al., 2009). For T5X-Base, we extend the official Google T5X release (commit: d3d3cbf) with sparsification training recipes and use Google TPUv3. We train these models from scratch using different training recipes across different patterns of N:M fine-grained structured sparsity. SR-STE (Zhou et al., 2021) serves as the baseline sparse training recipe to assess the effectiveness of the proposed training recipes in terms of model accuracy. Appendix C have details about training hyperparameters, dataset details, and evaluation metrics.

5.1. Image Classification \mapsto ViT-Base and SwinV2

ViT-Base model quality. Table 2 presents Top-1 validation accuracy for variations of N:M sparsity in ViT-Base, with the highest accuracy model indicated in bold. The “*Sparse Target*” column signifies the intended level of N:M sparsity. For example, a sparsity target of 1:32 indicates that sparse tensors exhibit at most one non-zero for every 32 contiguous elements. In low sparsity scenarios (e.g., 2:4 and 1:4), both MDGF and SR-STE demonstrate comparable performance. Nevertheless, with increases in either sparsity degree (e.g., 1:8 and higher) or the number of sparse layers, e.g., 1:4 (\mathcal{FF}) + 1:4 (\mathcal{QK}), employing SR-STE is detrimental to model quality. In contrast, the proposed decaying-based training

Table 1. The compute and memory contributions of the three major layers in Transformers. These estimations are made for ViT-Base. The FF layers account for around 64% of overall FLOPs and 66.6% of parameters. We use sequence length 196 to read image of 224x224.

	Einsum (Logit & Attend)	Projections (Q/K/V/O)	Feed Forward (FF1/FF2)
(T)FLOPs	1.42 (4%)	11.1 (32%)	22.20 (64%)
Params (MB)	0.0 (0%)	28.31 (33.3%)	56.62 (66.6%)

Table 2. ImageNet-1K Top-1 validation accuracy on ViT-Base across different N:M sparsity patterns and training recipes.

Sparse Target	Dense	SR-STE	MDGF-Linear	MDGF-Exponential	SDGF-Stepwise	SDGF-Geometric
2:4 (FF)	76.389	77.761	77.613	76.381	77.081	77.363
1:4 (FF)	76.389	78.782	78.512	78.579	77.357	78.347
1:8 (FF)	76.389	77.869	78.019	78.009	77.025	78.175
1:16 (FF)	76.389	75.637	76.594	77.325	75.923	76.869
1:32 (FF)	76.389	73.056	75.807	76.068	74.394	74.910
1:128 (FF)	76.389	72.069	74.012	74.180	71.725	69.801
1:4 (FF) + 1:4 (QK)	76.389	78.145	77.755	78.113	77.163	78.229
1:8 (FF) + 1:8 (QK)	76.389	75.527	76.473	77.349	76.617	76.334
1:8 (FF) + 1:4 (QK)	76.389	78.144	78.025	78.273	77.163	76.839
1:8 (FF) + 1:4 (QKV)	76.389	78.222	78.319	78.319	77.309	78.213

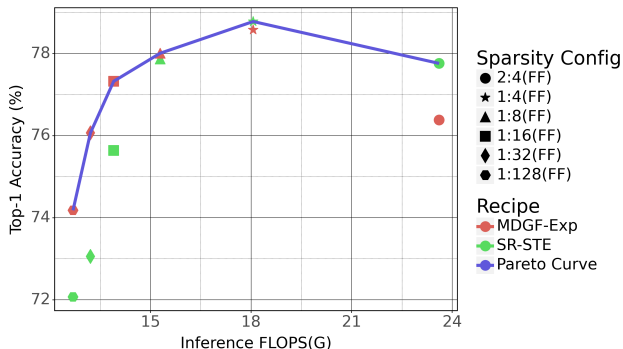


Figure 4. FLOP vs. Accuracy for ViT-Base+ImageNet-1K. recipes, MDGF and SDGF, yield the highest accuracy.

Interestingly, when aiming for a sparsity target of 1:32 (approximately 97%), MDGF-Exponential showcases a mere 0.3% reduction in accuracy compared to a fully dense model (76.389 vs. 76.068). Additionally, we notice that the model accuracy increases at modest sparsity degrees, specifically in 2:4/1:4/1:8 (FF) patterns, resulting in an improvement of up to $\Delta(Acc) = +2.4\%$ in 1:4 (FF). The increase in model accuracy, demonstrated in Figure 5(a), can be attributed to Occam’s Hill, wherein the positive impact of sparsity as a means of regularization is elucidated (Rasmussen & Ghahramani, 2001; Hoefler et al., 2021). The performance of MDGF-Exponential training recipe is comparable to that of SR-STE in low-sparsity scenarios. However, the proposed MDGF-Exponential recipe far surpasses SR-STE when confronted with high-sparsity patterns.

As commercially available accelerator can not support high-sparsity patterns. In order to assess the *potential* per-

formance benefits by comparing the savings in inference FLOPs as well as memory usage. Figure 4 visualizes the trade-off between accuracy and inference FLOPs across range of sparsity configurations and recipes. The results show that MDGF-Exponential with sparsity 1:16 provides similar accuracy as SR-STE 2:4 with 60% fewer inference FLOPs and 30% fewer parameters. Appendix E provides the details of FLOPs calculations.

SwinV2-Base model quality. Table 3 demonstrate Top-1 validation accuracy for SwinV2-Base. Similar to ViT-Base, we observe that the decaying-based algorithms outperforms SR-STE across various N:M sparsity patterns. In 1:4 and 1:8 (FF), SDGF-Geometric yields the highest Top-1 validation accuracy. Whereas, in high-sparsity patterns, MDGF-Exponential demonstrates superior performance compared to SR-STE. To summarize, the results from the two image classification models demonstrate that the proposed training recipes, MDGF and SDGF, which incorporate decaying-based approaches for N:M fine-grained structured sparsity, yield superior performance compared to SR-STE.

5.2. Language Understanding \leftrightarrow T5X-Base

We also analyze the efficacy of the proposed decaying-based training recipes for the language understanding task. We employ a dense pre-trained T5X-Base model trained on the C4 dataset with a span-corruption objective (Raffel et al., 2019). The dense pre-trained model undergoes fine-tuning using the GLUE dataset (Wang et al., 2019) with various training recipes for N:M structured sparsity.

Table 4 depicts the overall score, summarized across eight different GLUE tasks. We observe a consistent trend where

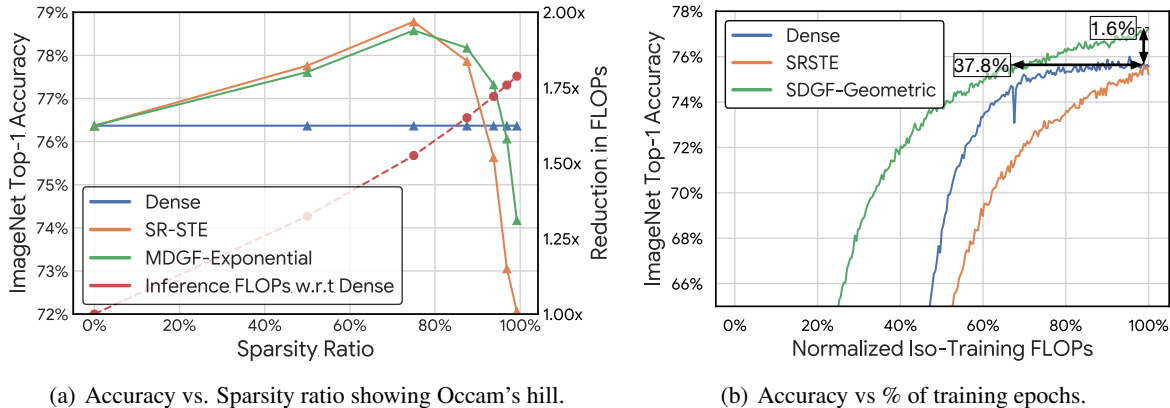


Figure 5. ViT-Base trained on ImageNet-1K with different sparsity patterns and targets. (a) shows the Occam’s hill where sparsity improves the model accuracy. The dashed red line shows the reduction in inference FLOPs at different sparsity ratio. At high sparsity regime ($>80\%$) MDGF yields better accuracy than SR-STE and (b) demonstrates model accuracy across training recipes (dense and sparse) at different training FLOPs. The vertical line indicates the proposed decaying method is better (1.6%) than dense model at given training FLOPs. The vertical line shows that the decaying based method reaches to dense model accuracy at 37.8% less training FLOPs.

Table 3. ImageNet-1K Top-1 validation accuracy on SwinV2-Base across different N:M sparse patterns and training recipes.

Sparse Target	Dense	SR-STE	MDGF-Exponential	SDGF-Stepwise	SDGF-Geometric
1:4 (FF)	83.45	82.355	82.491	82.267	82.469
1:8 (FF)	83.45	81.437	81.466	81.382	81.382
1:16 (FF)	83.45	80.154	80.542	80.386	80.274
1:32 (FF)	83.45	78.972	79.545	76.480	79.277
1:8 (FF) + 1:8(QK)	83.45	81.441	81.550	81.218	81.438

SDGF outperforms SR-STE at high-sparsity patterns and increasing number of sparse layers. Notably, we observe a relative difference of $\Delta = +5.3$ in 1:8 (FF) + 1:8 (QKV) sparsity pattern. Appendix A and Appendix B provide details about the T5X-Base model, per-task evaluation metrics, and additional ablation studies.

5.3. Language Translation \leftrightarrow Enc-Dec

Finally, we compare the performance of different sparse training recipes on WMT language translation task (Bojar et al., 2017). For that, we use an encoder-decoder transformer-based model (Vaswani et al., 2017) each with six layers and 16 heads, which is relatively smaller than T5X-Base. outlines the details about this model and the training hyperparameters.

Table 5 demonstrates the accuracy results across range of sparsity patterns and training recipes. We observe that SDGF and MDGF collectively outperform SR-STE across various N:M structured sparsity patterns. However, we note that the difference in accuracy achieved through different training recipes is relatively smaller. This can be attributed to the model size (6 layers vs. 12 layers in T5X-Base), as well as the nature of the translation task, which appears to be less

sensitive to sparsity patterns and training recipes³.

5.4. Baseline Comparison

SR-STE is our primary baseline in our evaluations as it has shown good results in low-sparsity regions [2:4,1:4] and is considered SOTA for N:M training. We also compared against other techniques like Inherited Dynamic Pruning (IDP) (Fang et al., 2022), and SNIP: Single-shot Network Pruning (Lee et al., 2019). Table 6 compares the results on T5X with GLUE dataset. We also tried to test against LBC (Zhang et al., 2022b) but could not recreate the results shown in the paper.⁴

5.5. Recipe impact for CNNs.

While the primary focus of this work is on evaluating sparse training recipe for transformer models, for the sake of completeness, we also test the efficacy of our recipe on CNNs. We train ResNet-50 following two sparse training recipes (SR-STE and MDGF-Exponential) and across differ-

³Model accuracy is less affected as we increase the sparsity level beyond 1:32.

⁴We have contacted the authors but cannot solve the issue.

Table 4. The GLUE overall score on the sparsified T5X-Base model across different N:M sparse training recipes and patterns.

Model	Sparsity Target	Dense	SR-STE	SDGF-Stepwise	SDGF-Geometric
T5X-Base	1:4 (FF)	86.2	84.1	83.7 ($\Delta = -0.4$)	83.4
T5X-Base	1:32 (FF)	86.2	79.4	80.9 ($\Delta = +1.5$)	79.3
T5X-Base	1:8 (FF) + 1:8 (QK)	86.2	75.8	80.7 ($\Delta = +4.9$)	76.8
T5X-Base	1:8 (FF) + 1:4(QKV)	86.2	78	80.3 ($\Delta = +2.3$)	78.9
T5X-Base	1:8 (FF) + 1:8 (QKV)	86.2	74.2	79.5 ($\Delta = +5.3$)	75.8

Table 5. The translation accuracy on WMT task across different N:M sparsity patterns and training recipes.

Model	Sparsity Target	Dense	SR-STE	SDGF-Stepwise	MDGF-Exponential
Enc-Dec (WMT)	1:16	0.747	0.709	0.717	0.717
Enc-Dec (WMT)	1:32	0.747	0.707	0.713	0.714
Enc-Dec (WMT)	1:64	0.747	0.707	0.710	0.711
Enc-Dec (WMT)	1:128	0.747	0.707	0.708	0.711

Table 6. Comparing various sparsification techniques by fine-tuning T5X on GLUE dataset.

Sparse Target	SR-STE (Zhou et al., 2021)	SNIP (Lee et al., 2019)	IDP (Fang et al., 2022)	MDGF-Exponential
1:32 (FF)	79.4		79.5	80.6
				80.9

ent sparse patterns (2:8, 1:8). We pruned all the convolution layers and evaluate Top-1 validation accuracy on CIFAR-10. Table 7 shows a similar pattern, decaying-based sparse training recipes outperform SR-STE in both cases.

Table 7. ResNet-50 Top-1 validation accuracy.

Sparse Target	Dense	SR-STE	MDGF-Exponential
2:8	85.09	83.33	83.60
1:8	85.09	80.78	82.48

6. Limitations and Future Works

The prevalence of self-attention models and their growing parameter size inspired this work. The primary objective of this research is to enable effective sparsity (acceptable quality) with high ratio for such models. While in this paper, we evaluate the proposed sparse training recipes in isolation (either MDGF or SDGF), combining these methods at different training region can potentially lead to higher model quality. The main finding of our work is that pruning in the high sparsity regime adversely affects gradient estimation, consequently resulting in suboptimal model quality. To mitigate this undesired phenomenon, we propose a strategy of progressively tightening the gradient flow for pruned weights. Our results show that this idea, while simple, proves to be effective across a variety of models and datasets.

7. Conclusion

This work studies the efficacy of recent sparsity recipes for N:M sparsity across range of transformer-based models. We observe that conventional methods introduce nontrivial noise to gradient estimates, particularly at high-sparsity regimes ($>75\%$). Building on this observation, we propose and compare a class of decaying-based training recipes for N:M structured sparsity. Our results demonstrate that our recipe, MDGF-Exponential, consistently deliver SOTA model accuracy for a variety of vision and language models, with more than $\sim 2\%$ (vision) and $\sim 5\%$ (language) improvement at high sparsity regime. We empirically show that the effectiveness of the proposed recipes primarily depending on the gradient flow, especially at the initial training steps. Finally, we compare the sparse training recipes in terms training and inference FLOPs. At iso-FLOPs for training, our approach offers 2% higher accuracy. In addition, we demonstrate that MDGF-Exponential (1:16) yields comparable accuracy to SR-STE (2:4), resulting in approximately 60% fewer inference FLOPs and 30% fewer parameters.

Acknowledgements

We would like to extend our gratitude towards Jeremiah Willcock, Penporn Koanantakool, Chandu Thekkath, Cliff Young, and James Laudon for their invaluable feedback on the early draft of this work. We also appreciate the support from our extended team at Google DeepMind.

Bibliography

- Akhlaghi, V., Yazdanbakhsh, A., Samadi, K., Gupta, R. K., and Esmaeilzadeh, H. Snapea: Predictive Early Activation for Reducing Computation in Deep Convolutional Neural Networks. In *ISCA*, 2018.
- Anil, R., Borgeaud, S., Wu, Y., Alayrac, J.-B., Yu, J., Soricut, R., Schalkwyk, J., Dai, A. M., Hauth, A., et al. Gemini: A Family of Highly Capable Multimodal Models. *arXiv preprint arXiv:2312.11805*, 2023.
- Bambhaniya, A. R., Yazdanbakhsh, A., Subramanian, S., and Krishna, T. Accelerating attention based models via hw-sw co-design using fine-grained sparsification. In *Architecture and System Support for Transformer Models (ASSYST@ ISCA 2023)*, 2023.
- Bellec, G., Kappel, D., Maass, W., and Legenstein, R. Deep Rewiring: Training very Sparse Deep Networks. In *ICLR*, 2018.
- Beltagy, I., Peters, M. E., and Cohan, A. Longformer: The Long-Document Transformer. *arXiv preprint arXiv:2004.05150*, 2020.
- Bojar, O., Chatterjee, R., Federmann, C., Graham, Y., Hadrow, B., Huang, S., Huck, M., Koehn, P., Liu, Q., Logacheva, V., Monz, C., Negri, M., Post, M., Rubino, R., Specia, L., and Turchi, M. Findings of the 2017 Conference on Machine Translation (WMT17). In *Proceedings of the Second Conference on Machine Translation, Volume 2: Shared Task Papers*, 2017.
- Child, R., Gray, S., Radford, A., and Sutskever, I. Generating Long Sequences with Sparse Transformers. *arXiv preprint arXiv:1904.10509*, 2019.
- Deng, J., Dong, W., Socher, R., Li, L.-J., Li, K., and Fei-Fei, L. ImageNet: A Large-Scale Hierarchical Image Database. In *CVPR*, 2009.
- Dettmers, T. and Zettlemoyer, L. Sparse Networks from Scratch: Faster Training without Losing Performance. *arXiv preprint arXiv:1907.04840*, 2019.
- Devlin, J., Chang, M.-W., Lee, K., and Toutanova, K. Bert: Pre-training of deep bidirectional transformers for language understanding, 2019.
- Dosovitskiy, A., Beyer, L., Kolesnikov, A., Weissenborn, D., Zhai, X., Unterthiner, T., Dehghani, M., Minderer, M., Heigold, G., Gelly, S., et al. An Image is Worth 16x16 Words: Transformers for Image Recognition at Scale. In *ICLR*, 2021.
- Elsen, E., Dukhan, M., Gale, T., and Simonyan, K. Fast Sparse ConvNets. In *CVPR*, 2020.
- Evci, U., Pedregosa, F., Gomez, A., and Elsen, E. The Difficulty of Training Sparse Neural Networks. *arXiv preprint arXiv:1906.10732*, 2019.
- Evci, U., Gale, T., Menick, J., Castro, P. S., and Elsen, E. Rigging the lottery: Making all tickets winners. In *ICML*, 2020.
- Fang, C., Zhou, A., and Wang, Z. An algorithm–hardware co-optimized framework for accelerating n:m sparse transformers. *IEEE Transactions on Very Large Scale Integration (VLSI) Systems*, 30(11):1573–1586, nov 2022. doi: 10.1109/tvlsi.2022.3197282. URL <https://doi.org/10.1109/tvlsi.2022.3197282>.
- Frankle, J. and Carbin, M. The Lottery Ticket Hypothesis: Finding Sparse, Trainable Neural Networks. In *ICLR*, 2019.
- Frankle, J., Dziugaite, G. K., Roy, D. M., and Carbin, M. Pruning Neural Networks at Initialization: Why are We Missing the Mark? *arXiv preprint arXiv:2009.08576*, 2020.
- Frantar, E. and Alistarh, D. SparseGPT: Massive Language Models Can Be Accurately Pruned in One-Shot, 2023.
- Gale, T., Elsen, E., and Hooker, S. The State of Sparsity in Deep Neural Networks. *arXiv preprint arXiv:1902.09574*, 2019.
- Gamboia, N., Kudrolli, K., Dhoot, A., and Pedram, A. Campfire: Compressible, Regularization-Free, Structured Sparse Training for Hardware Accelerators. *arXiv preprint arXiv:2001.03253*, 2020.
- Gou, J., Yu, B., Maybank, S. J., and Tao, D. Knowledge Distillation: A Survey. *International Journal of Computer Vision*, 2021.
- Gray, S., Radford, A., and Kingma, D. P. GPU Kernels for Block-Sparse Weights. *arXiv preprint arXiv:1711.09224*, 3:2, 2017.
- Guo, Y., Yao, A., and Chen, Y. Dynamic Network Surgery for Efficient DNNs. In *NeurIPS*, 2016.
- Han, S., Mao, H., and Dally, W. J. Deep Compression: Compressing Deep Neural Networks with Pruning, Trained Quantization and Huffman Coding. *arXiv preprint arXiv:1510.00149*, 2015a.
- Han, S., Pool, J., Tran, J., and Dally, W. Learning both Weights and Connections for Efficient Neural Network. In *NeurIPS*, 2015b.
- He, Y., Zhang, X., and Sun, J. Channel Pruning for Accelerating Very Deep Neural Networks. In *ICCV*, 2017.
- Hoefler, T., Alistarh, D., Ben-Nun, T., Dryden, N., and Peste, A. Sparsity in Deep Learning: Pruning and Growth for Efficient Inference and Training in Neural Networks, 2021.
- Jaszczur, S., Chowdhery, A., Mohiuddin, A., Łukasz Kaiser, Gajewski, W., Michalewski, H., and Kanerva, J. Sparse is Enough in Scaling Transformers. In *NeurIPS*, 2021.
- Jeong, G., Damani, S., Bambhaniya, A. R., Qin, E., Hughes, C. J., Subramoney, S., Kim, H., and Krishna, T. Vegeta: Vertically-integrated extensions for sparse/dense gemm tile acceleration on cpus. In *2023 IEEE International Symposium on High-Performance Computer Architecture (HPCA)*, pp. 259–272, 2023. doi: 10.1109/HPCA56546.2023.10071058.
- Johnson, R. and Zhang, T. Accelerating Stochastic Gradient Descent Using Predictive Variance Reduction. In

- NeurIPS*, 2013.
- Kang, H.-J. Accelerator-Aware Pruning for Convolutional Neural Networks. *IEEE Transactions on Circuits and Systems for Video Technology*, 2019.
- Kim, S., Gholami, A., Yao, Z., Mahoney, M. W., and Keutzer, K. I-BERT: Integer-only BERT Quantization. *arXiv preprint arXiv:2101.01321*, 2021.
- Kitaev, N., Łukasz Kaiser, and Levskaya, A. Reformer: The Efficient Transformer. *arXiv preprint arXiv:2001.04451*, 2020.
- Krizhevsky, A., Hinton, G., et al. Learning Multiple Layers of Features from Tiny Images. Technical report, Citeseer, 2009.
- Kusupati, A., Ramanujan, V., Somani, R., Wortsman, M., Jain, P., Kakade, S., and Farhadi, A. Soft threshold weight reparameterization for learnable sparsity. In *ICML*, 2020.
- LeCun, Y., Denker, J., and Solla, S. Optimal brain damage. *NeurIPS*, 1989.
- Lee, N., Ajanthan, T., and Torr, P. H. SNIP: Single-shot Network Pruning based on Connection Sensitivity. In *ICLR*, 2019.
- Li, C., Awan, A. A., Tang, H., Rajbhandari, S., and He, Y. 1-bit LAMB: Communication Efficient Large-scale Large-batch Training with LAMB’s Convergence Speed. In *HiPC*, 2022.
- Li, H., Kadav, A., Durdanovic, I., Samet, H., and Graf, H. P. Pruning Filters for Efficient ConvNets. *arXiv preprint arXiv:1608.08710*, 2016.
- Lin, M., Cao, L., Li, S., Ye, Q., Tian, Y., Liu, J., Tian, Q., and Ji, R. Filter Sketch for Network Pruning. *TNNLS*, 2021.
- Liu, Z., Sun, M., Zhou, T., Huang, G., and Darrell, T. Rethinking the Value of Network Pruning. *arXiv preprint arXiv:1810.05270*, 2018.
- Liu, Z., Hu, H., Lin, Y., Yao, Z., Xie, Z., Wei, Y., Ning, J., Cao, Y., Zhang, Z., Dong, L., Wei, F., and Guo, B. Swin Transformer V2: Scaling Up Capacity and Resolution. In *CVPR*, 2022a.
- Liu, Z., Whatmough, P. N., Zhu, Y., and Mattina, M. S2ta: Exploiting structured sparsity for energy-efficient mobile cnn acceleration. In *2022 IEEE International Symposium on High-Performance Computer Architecture (HPCA)*, pp. 573–586, Los Alamitos, CA, USA, apr 2022b. IEEE Computer Society. doi: 10.1109/HPCA53966.2022.00049. URL <https://doi.ieeecomputersociety.org/10.1109/HPCA53966.2022.00049>.
- Lu, Y., Li, C., Zhang, M., De Sa, C., and He, Y. Maximizing communication Efficiency for Large-scale Training via 0/1 Adam. *arXiv preprint arXiv:2202.06009*, 2022.
- Lu, Y., Agrawal, S., Subramanian, S., Rybakov, O., Sa, C. D., and Yazdanbakhsh, A. STEP: Learning N:M Structured Sparsity Masks from Scratch with Precondition. In *ICML*, 2023.
- Ma, X., Lin, S., Ye, S., He, Z., Zhang, L., Yuan, G., Tan, S. H., Li, Z., Fan, D., Qian, X., Lin, X., Ma, K., and Wang, Y. Non-Structured DNN Weight Pruning – Is It Beneficial in Any Platform? *IEEE transactions on neural networks and learning systems*, 2021.
- Mishra, A., Latorre, J. A., Pool, J., Stolic, D., Stolic, D., Venkatesh, G., Yu, C., and Micikevicius, P. Accelerating Sparse Deep Neural Networks. *arXiv preprint arXiv:2104.08378*, 2021.
- Mocanu, D. C., Mocanu, E., Stone, P., Nguyen, P. H., Gibescu, M., and Liotta, A. Scalable Training of Artificial Neural Networks with Adaptive Sparse Connectivity Inspired by Network Science. *Nature communications*, 2018.
- Molchanov, P., Tyree, S., Karras, T., Aila, T., and Kautz, J. Pruning Convolutional Neural Networks for Resource Efficient Inference. *arXiv preprint arXiv:1611.06440*, 2016.
- Molchanov, P., Mallya, A., Tyree, S., Frosio, I., and Kautz, J. Importance Estimation for Neural Network Pruning. In *CVPR*, 2019.
- Narang, S., Elsen, E., Diamos, G., and Sengupta, S. Exploring Sparsity in Recurrent Neural Networks. *arXiv preprint arXiv:1704.05119*, 2017a.
- Narang, S., Undersander, E., and Diamos, G. Block-Sparse Recurrent Neural Networks. *arXiv preprint arXiv:1711.02782*, 2017b.
- Nvidia. NVIDIA Ampere Architecture Whitepaper. <https://images.nvidia.com/aem-dam/en-zz/Solutions/data-center/nvidia-ampere-architecture-whitepaper.pdf>, 2021a.
- Nvidia. NVIDIA ASP (Automatic Sparsity). <https://github.com/NVIDIA/apex/tree/master/apex/contrib/sparsity>, 2021b.
- OpenAI. GPT-4 Technical Report, 2023.
- Pan, Y., Yu, J., Lukefahr, A., Das, R., and Mahlke, S. Bit-SET: Bit-Serial Early Termination for Computation Reduction in Convolutional Neural Networks. *ACM Transactions on Embedded Computing Systems*, 2023.
- Parashar, A., Rhu, M., Mukkara, A., Puglielli, A., Venkatesan, R., Khailany, B., Emer, J., Keckler, S. W., and Dally, W. J. Senn: An accelerator for compressed-sparse convolutional neural networks. *ACM SIGARCH Computer Architecture News*, 45(2):27–40, 2017.
- Pool, J. and Yu, C. Channel Permutations for N: M Sparsity. *NeurIPS*, 2021.
- Qin, E., Jeong, G., Won, W., Kao, S.-C., Kwon, H., Srinivasan, S., Das, D., Moon, G. E., Rajamanickam, S., and Krishna, T. Extending Sparse Tensor Accelerators to Support Multiple Compression Formats. In *IPDPS*, 2021.
- Qin, E., Garg, R., Bambhaniya, A., Pellauer, M., Parashar, A., Rajamanickam, S., Hao, C., and Krishna, T. Enabling flexibility for sparse tensor acceleration via heterogeneity, 2022.
- Raffel, C., Shazeer, N., Roberts, A., Lee, K., Narang, S.,

- Matena, M., Zhou, Y., Li, W., and Liu, P. J. Exploring the Limits of Transfer Learning with a Unified Text-to-Text Transformer. *arXiv preprint arXiv:1910.10683*, 2019.
- Rasmussen, C. and Ghahramani, Z. Occam’s Razor. *NeurIPS*, 2001.
- Renda, A., Frankle, J., and Carbin, M. Comparing Rewinding and Fine-tuning in Neural Network Pruning. In *ICLR*, 2020.
- Roy, A., Saffar, M., Vaswani, A., and Grangier, D. Efficient Content-based Sparse Attention with Routing Transformers. *TACL*, 2021.
- Shen, S., Dong, Z., Ye, J., Ma, L., Yao, Z., Gholami, A., Mahoney, M. W., and Keutzer, K. Q-BERT: Hessian Based Ultra Low Precision Quantization of BERT. In *AAAI*, 2020.
- Tang, H., Gan, S., Awan, A. A., Rajbhandari, S., Li, C., Lian, X., Liu, J., Zhang, C., and He, Y. 1-bit Adam: Communication Efficient Large-scale Training with Adam’s Convergence Speed. In *ICLR*, 2021.
- Tay, Y., Dehghani, M., Bahri, D., and Metzler, D. Efficient Transformers: A Survey. *ACM Comput. Surv.*, dec 2022.
- Tessier, H., Gripon, V., Léonardon, M., Arzel, M., Hannagan, T., and Bertrand, D. Rethinking Weight Decay for Efficient Neural Network Pruning. *Journal of Imaging*, 2022.
- Touvron, H., Martin, L., Stone, K., Albert, P., Almahairi, A., Babaei, Y., Bashlykov, N., Batra, S., Bhargava, P., Bhosale, S., et al. Llama 2: Open Foundation and Fine-Tuned Chat Models. *arXiv preprint arXiv:2307.09288*, 2023.
- Vaswani, A., Shazeer, N., Parmar, N., Uszkoreit, J., Jones, L., Gomez, A. N., Kaiser, Ł., and Polosukhin, I. Attention is All You Need. In *NeurIPS*, 2017.
- Wang, A., Singh, A., Michael, J., Hill, F., Levy, O., and Bowman, S. R. GLUE: A Multi-Task Benchmark and Analysis Platform for Natural Language Understanding. *arXiv preprint arXiv:1804.07461*, 2019.
- Wang, C., Chen, X., Smola, A. J., and Xing, E. P. Variance Reduction for Stochastic Gradient Optimization. In *NeurIPS*, 2013.
- Wei, J., Tay, Y., Bommasani, R., Raffel, C., Zoph, B., Borgeaud, S., Yogatama, D., Bosma, M., Zhou, D., Metzler, D., Chi, E. H., Hashimoto, T., Vinyals, O., Liang, P., Dean, J., and Fedus, W. Emergent Abilities of Large Language Models. *TMLR*, 2022.
- Wen, W., Wu, C., Wang, Y., Chen, Y., and Li, H. Learning Structured Sparsity in Deep Neural Networks. *NeurIPS*, 2016.
- Wightman, R. PyTorch Image Models. <https://github.com/rwightman/pytorch-image-models>, 2019.
- Wortsman, M., Farhadi, A., and Rastegari, M. Discovering Neural Wirings. In *NeurIPS*, 2019.
- Yao, Z., Cao, S., Xiao, W., Zhang, C., and Nie, L. Balanced Sparsity for Efficient DNN Inference on GPU. In *AAAI*, 2019.
- Yeom, S.-K., Seegerer, P., Lapuschkin, S., Binder, A., Wiedemann, S., Müller, K.-R., and Samek, W. Pruning by Explaining: A Novel Criterion for Deep Neural Network Pruning. *Pattern Recognition*, 2021.
- Zafir, O., Boudoukh, G., Izsak, P., and Wasserblat, M. Q8BERT: Quantized 8Bit BERT. *arXiv preprint arXiv:1910.06188*, 2019.
- Zhang, S., Roller, S., Goyal, N., Artetxe, M., Chen, M., Chen, S., Dewan, C., Diab, M., Li, X., Lin, X. V., Mihaylov, T., Ott, M., Shleifer, S., Shuster, K., Simig, D., Koura, P. S., Sridhar, A., Wang, T., and Zettlemoyer, L. OPT: Open Pre-trained Transformer Language Models. *arXiv preprint arXiv:2205.01068*, 2022a.
- Zhang, W., Hou, L., Yin, Y., Shang, L., Chen, X., Jiang, X., and Liu, Q. TernaryBERT: Distillation-aware Ultra-low Bit BERT. *arXiv preprint arXiv:2009.12812*, 2020.
- Zhang, Y., Lin, M., Lin, Z., Luo, Y., Li, K., Chao, F., Wu, Y., and Ji, R. Learning best combination for efficient n:m sparsity, 2022b.
- Zhou, A., Ma, Y., Zhu, J., Liu, J., Zhang, Z., Yuan, K., Sun, W., and Li, H. Learning N:M Fine-grained Structured Sparse Neural Networks from Scratch. In *ICLR*, 2021.
- Zhu, M. and Gupta, S. To Prune, or not to Prune: Exploring the Efficacy of Pruning for Model Compression. *arXiv preprint arXiv:1710.01878*, 2017.
- Zhu, M., Zhang, T., Gu, Z., and Xie, Y. Sparse Tensor Core: Algorithm and Hardware Co-design for Vector-wise Sparse Neural Networks on Modern GPUs. In *MICRO*, 2019.

A. Ablations Studies

This section shows the various ablation studies we performed during our experiments.

A.1. Effect of dense training steps (d)

Both our proposed methods, MDGF and SDGF include a dense training phase. We do an ablation study on different amounts of dense training steps(% of total steps) in Table 8. We perform this study on the language translation model (more implementation details in section §C.2.4) trained on WMT-17. We found that changing the dense step between 1.25% - 10% of the total training steps does not observably change the accuracy performance. However, empirically, we found that the dense training phase is still essential. The model cannot achieve as competitive accuracy without few epochs of dense training.

Table 8. Ablation: The effect of number of dense training steps (d).

Accuracy		MDGF-Linear				SDGF-Stepwise			
Sparsity Target		1:16	1:32	1:64	1:128	1:16	1:32	1:64	1:128
Dense steps (d)	1.25%	0.7155	0.7134	0.7106	0.7100	0.7157	0.7134	0.7108	0.7106
	2.5%	0.7160	0.7127	0.7110	0.7093	0.7160	0.7136	0.7117	0.7100
	5%	0.7157	0.7137	0.7103	0.7094	0.7164	0.7141	0.7107	0.7098
	10%	0.7156	0.7126	0.7107	0.7104	0.7165	0.7128	0.7115	0.7107

A.2. Effects of fine-tuning steps (s)

We also have a sets of study on number of fine-tuning steps in Table 9. We perform this study on the language translation model (more implementation details in section §C.2.4) trained on WMT-17. We found that for all of our proposed methods, the fine-tuning steps between 10% - 20% of the total training steps do not observably change the accuracy performance. However, empirically, we also found few steps of fine-tuning at the end are essential to recovering the accuracy.

Table 9. Ablation: The effect of number of fine-tuning steps (s).

Accuracy		MDGF-Linear				SDGF-Stepwise			
Sparsity Target		1:16	1:32	1:64	1:128	1:16	1:32	1:64	1:128
Fine-tuning steps (s)	10%	0.7153	0.7130	0.7107	0.7098	0.7160	0.7125	0.7095	0.7072
	20%	0.7161	0.7132	0.7106	0.7097	0.7121	0.7093	0.7081	0.7065

A.3. Effect of (β^t) in MDGF-Linear

We also study on effect of decay rate on model’s accuracy in Table 10. We do experiments with varying β^t for ViT-Base trained on Imagenet-1k for different sparsity targets.

We observe that a higher decay rate is beneficial at low sparsity targets (2:4,1:4), but for targets higher than 1:8, we found lower decay rate works better.

Table 10. Ablation: The effect of mask decay rate (β^t) for MDGF-Linear.

Sparsity Target		2:4	1:4	1:8
Mask decay rate (β^t)	0.0002	77.495	78.448	78.019
	0.001	77.613	78.512	76.4075

B. Detailed Results for T5X-Base Sparsification on GLUE Dataset

We compared sparsification methods N:M block sparsification against state-of-the-art technique, SR-STE on. T5 model uses a span-based masked language modeling (MLM) objective. T5 models were introduced in (Raffel et al., 2019) and the updated models are available at T5X-github. We train a pre trained t5x-base model on GLUE dataset (Wang et al., 2019).

The main paper shows a snapshot of the performance across various sparsity targets using the overall score as metric. Table 11 presents all 9 scores for each sparsification technique and sparsity target.

Progressive Gradient Flow for Robust N:M Sparsity Training in Transformers

Table 11. GLUE full score using various T5X-base with different N:M sparse targets and various sparsification techniques.

		overall score	CoLA	MNLI matched	MNLI mismatched	MRPC	QNLI	QQP	RTE	SST-2	STS-B
Dense	-	86.2	58.9	87.2	87	92.4 / 89.2 (90.8)	93.6	92.0 / 89.2 (90.6)	82.3	95	90.1 / 90.0 (90.0)
SR-STE (Zero Dense)	1:4	83.1	41.8	85.2	85.3	92.8 / 90.0 (91.4)	92.3	91.8 / 88.9 (90.3)	79.1	93.6	89.5 / 89.2 (89.3)
SR-STE (10K Dense)	1:4	84.1	48.1	85.7	85.6	92.4 / 89.5 (91.0)	92.1	91.8 / 89.0 (90.4)	82.7	93.6	87.9 / 87.7 (87.8)
MdGF-Stepwise (10K Dense)	1:4	83.7	48.8	85.3	85.4	92.4 / 89.2 (90.8)	92.3	91.8 / 89.0 (90.4)	80.5	93.5	86.5 / 86.3 (86.4)
MdGF-Geometric (Zero Dense)	1:4	83.3	48.4	85.3	85.3	92.0 / 89.0 (90.5)	91.8	91.8 / 88.9 (90.3)	78	92.8	87.3 / 87.4 (87.3)
MdGF-Geometric (10K Dense)	1:4	83.4	47.2	85.4	85.3	92.6 / 89.7 (91.1)	92	91.8 / 89.0 (90.4)	79.8	92.9	86.7 / 86.4 (86.5)
SR-STE (Zero Dense)	1:32	77.1	19	81.3	81.3	90.9 / 87.0 (89.0)	86.9	90.6 / 87.4 (89.0)	71.1	89.9	86.7 / 86.8 (86.8)
SR-STE (10K Dense)	1:32	79.4	29.4	82.2	82.6	91.5 / 88.5 (90.0)	89.6	91.2 / 88.2 (89.7)	72.6	91.4	87.1 / 87.2 (87.2)
MdGF-Stepwise (10K Dense)	1:32	80.9	38.3	83.6	83.7	92.5 / 89.7 (91.1)	90.5	91.5 / 88.5 (90.0)	74.4	91.2	85.2 / 85.0 (85.1)
MdGF-Geometric (Zero Dense)	1:32	77.6	20.2	81.3	81.6	91.8 / 88.5 (90.1)	87.2	90.8 / 87.7 (89.2)	73.3	90.1	85.8 / 85.5 (85.6)
MdGF-Geometric (10K Dense)	1:32	79.3	29.2	82.3	82.9	91.3 / 88.0 (89.6)	90.4	91.3 / 88.3 (89.8)	73.3	90.5	85.4 / 85.4 (85.4)
SR-STE (Zero Dense)	1:8(FF) + 1:8(QK)	74.4	15.7	77.2	77.6	89.9 / 85.8 (87.8)	83.6	89.7 / 86.2 (87.9)	67.5	88.2	84.1 / 83.9 (84.0)
SR-STE (10K Dense)	1:8(FF) + 1:8(QK)	75.8	19.9	78.6	79.4	89.7 / 86.0 (87.9)	84	90.1 / 86.7 (88.4)	70	89.4	84.5 / 84.2 (84.4)
MdGF-Stepwise (10K Dense)	1:8(FF) + 1:8(QK)	80.7	38.7	83.1	83.2	90.9 / 87.7 (89.3)	89.9	91.2 / 88.2 (89.7)	76.2	91.9	84.5 / 84.5 (84.5)
MdGF-Geometric (Zero Dense)	1:8(FF) + 1:8(QK)	75.8	21.6	78.8	79	90.0 / 86.0 (88.0)	83.6	90.1 / 86.6 (88.3)	69.7	88.9	84.0 / 83.9 (83.9)
MdGF-Geometric (10K Dense)	1:8(FF) + 1:8(QK)	76.8	22.3	80.7	80.9	89.8 / 85.8 (87.8)	86.3	90.5 / 87.4 (89.0)	70	91.1	83.7 / 83.4 (83.6)
SR-STE (Zero Dense)	1:8(FF) + 1:8(QKV)	73.2	13.5	76.3	76.4	89.0 / 84.6 (86.8)	83.2	89.5 / 85.9 (87.7)	63.9	87	84.3 / 84.2 (84.2)
SR-STE (10K Dense)	1:8(FF) + 1:8(QKV)	74.2	16.1	77.7	77.6	88.5 / 84.1 (86.3)	82.9	89.9 / 86.3 (88.1)	66.4	88.8	84.4 / 84.2 (84.3)
MdGF-Stepwise (10K Dense)	1:8(FF) + 1:8(QKV)	79.5	33	82.3	82.3	91.3 / 87.7 (89.5)	89.2	91.0 / 88.0 (89.5)	74.4	91.1	84.5 / 84.8 (84.6)
MdGF-Geometric (Zero Dense)	1:8(FF) + 1:8(QKV)	75.5	22.1	78.6	78.7	90.5 / 86.8 (88.6)	83.4	90.0 / 86.5 (88.2)	67.9	88.2	84.2 / 84.2 (84.2)
MdGF-Geometric (10K Dense)	1:8(FF) + 1:8(QKV)	75.8	19.5	79.4	79.6	89.4 / 85.3 (87.3)	84.5	90.2 / 86.8 (88.5)	70.4	89.8	83.3 / 83.0 (83.2)
SR-STE (Zero Dense)	1:8(FF) + 1:4(QKV)	75.1	15	78.4	79	90.5 / 86.8 (88.6)	84.2	90.1 / 86.6 (88.4)	67.9	88.4	86.2 / 86.1 (86.2)
SR-STE (10K Dense)	1:8(FF) + 1:4(QKV)	78	24.5	81.2	81.6	91.1 / 87.7 (89.4)	87.1	90.6 / 87.3 (89.0)	72.2	90.9	85.8 / 85.8 (85.8)
MdGF-Stepwise (10K Dense)	1:8(FF) + 1:4(QKV)	80.3	36.4	83.2	83.4	90.9 / 87.3 (89.1)	90.3	91.3 / 88.3 (89.8)	74.7	90.9	85.2 / 85.0 (85.1)
MdGF-Geometric (Zero Dense)	1:8(FF) + 1:4(QKV)	76.8	20.2	80.5	80.8	91.3 / 87.7 (89.5)	85.4	90.3 / 87.0 (88.6)	70.8	90.4	84.9 / 84.9 (84.9)
MdGF-Geometric (10K Dense)	1:8(FF) + 1:4(QKV)	78.9	27.7	82.4	82.4	91.3 / 87.7 (89.5)	88.8	91.0 / 88.1 (89.6)	74.4	91.3	84.5 / 84.5 (84.5)

Here is an itemized list of nine tasks used in the GLUE dataset, along with brief descriptions of each:

- **CoLA (Corpus of Linguistic Acceptability)**: Classify whether a given sentence is grammatically acceptable or not.
- **MNLI (Multi-Genre Natural Language Inference)**: Classify the relationship between a given premise and hypothesis as entailment, contradiction, or neutral. We use the standard test set, for which we obtained private labels from the authors, and evaluate on both the matched (in-domain) and mismatched (cross-domain) sections.
- **MRPC (Microsoft Research Paraphrase Corpus)**: Determine whether a pair of sentences express the same meaning or not.
- **QNLI (Question-answering Natural Language Inference)**: Determine whether a given question can be answered correctly using a given sentence.
- **QQP (Quora Question Pairs)**: Determine whether a pair of questions from Quora are semantically equivalent or not.
- **RTE (Recognizing Textual Entailment)**: Classify the relationship between a given premise and hypothesis as entailment or not.
- **SST-2 (Stanford Sentiment Treebank)**: Determine the sentiment of a given sentence as either positive or negative.
- **STS-B (Semantic Textual Similarity Benchmark)**: Calculate the similarity score between two sentences on a scale from 0 to 5.

These tasks cover various aspects of language understanding, including sentence acceptability, sentiment analysis, paraphrase detection, textual similarity, natural language inference, question-answering, and co-reference resolution.

Figure 7 shows the accuracy vs. fine-tuning step curve for each of the 9 benchmarks of GLUE.

C. Detailed Experimental Settings

C.1. Datasets

C.1.1. IMAGENET-1K

ImageNet-1K (Deng et al., 2009) is a large-scale image classification task, known as one of the most challenging image classification benchmarks. It consists of more than 1.2 million training images and 50K validation images with a size of 224x224 pixels, each with 3 channels. Each image is labeled as one of the 1K classes. We use this dataset for studies in

Section 4.1 of the main paper. For ViT and SwinV2 experiments, we use a patch size of 16. This converts the 224x224 pixel image into an input of sequence length $224/16 * 224/16 = 196$.

Evaluation metrics. All reported results follow standard Top-1 validation accuracy.

C.1.2. CIFAR10

CIFAR-10 (Krizhevsky et al., 2009) is a smaller-scale image classification dataset consisting of 10 classes. Each class has 6000 color images of 32x32 pixels in size.

Evaluation metrics. All reported results to follow standard Top-1 accuracy.

C.1.3. GLUE

The General Language Understanding Evaluation (GLUE) (Wang et al., 2019) benchmark is a collection of resources for training, evaluating, and analyzing natural language understanding systems. GLUE consists of: A benchmark of nine sentence- or sentence-pair language understanding tasks built on established existing datasets and selected to cover a diverse range of dataset sizes, text genres, and degrees of difficulty, Table 11 shows the overall score for each sparsity target using different sparsification methods.

Evaluation metrics. All reported results in the main paper use the overall average score.

C.1.4. WMT

WMT-17 (English-German) (Bojar et al., 2017) is a key benchmark in machine translation research. They hold several translation datasets across different languages. The training set consists of about 4.5 million bilingual sentence pairs from WMT 2014.

Evaluation metrics. We calculate accuracy by comparing the translated output to the correct translation in the validation datasets.

C.2. Hyperparameters for Different Models

C.2.1. IMAGE CLASSIFICATION → VISION TRANSFORMERS (ViT)

We train the ViT-Base model on ImageNet-1k with hyperparameters presented in Table 12. We follow the hyperparameter setting in (Wightman, 2019) for all ViT experiments. We also use the same hyperparameters to train ViT-Tiny model (3 layers, 3 attention head per layer, Embedding dimension: 192) on CIFAR-10 for initial experiments in Section 3.2 for analysing the trends of weights, gradients and optimizer moments and comparing those with SR-STE.

Table 12. Hyperparameters used for training ViT on ImageNet-1K.

Batch Size	256
Training Epoches	350
Learning Rate	1e-3
LR Warmup Epoches	15
LR Decay scheduler	Cosine
Decay Rate	0.1
Decay Epoches	100
Optimizer	AdamW
Optimizer coefs	beta1 = 0.9, beta2 = 0.999

The detailed list of all hyperparameters can be found at hyperparaters.yaml. For ViT-Base, the training phase takes ≈ 44 hours on 16 - A100 GPUs.

Figure 6 shows the Top-1 and Top-5 accuracy trends for training ViT to various sparsity targets with different sparsification techniques. We observe generally, MDGF and SDGF are better than SR-STE, especially for high-sparsity targets.

C.2.2. IMAGE CLASSIFICATION → SWIN TRANSFORMER V2 (SwinV2)

We train the SwinV2-Base model on imagenet-1k with hyperparameters presented in Table 13. We follow the hyperparameter setting in (Liu et al., 2022a) for all SwinV2 experiments.

Table 13. Hyperparameters used for training SwinV2 on ImageNet-1K.

Batch Size	128
Training Epoches	350
Learning Rate	1e-3
LR Warmup Epoches	20
LR Decay scheduler	Cosine
Decay Rate	0.1
Decay Epoches	30
Optimizer	AdamW
Optimizer coefs	beta1 = 0.9, beta2 = 0.999

The detailed model configuration is the same as present in the original Microsoft research GitHub repo, SwinV2-base.yaml. The detailed list of all hyperparameters was taken from config.yaml. For SwinV2-Base, the training phase takes ≈ 54 hours on 16 - A100 GPUs.

C.2.3. LANGUAGE UNDERSTANDING → T5X

We train the T5X-Base model on GLUE dataset with hyperparameters presented in Table 14. We follow the hyperparameter setting in (Raffel et al., 2019) for all T5X training experiments.

The detailed model configuration is the same as present in the original Google research GitHub repo, T5X model T5X-Base’s training phase takes ≈ 22 hours on 8×Google Cloud TPUv3 cores.

Table 14. Hyperparameters used for training T5X on GLUE.

Batch Size	128
Training Steps	100k
Learning Rate	1e-3
LR Warmup Steps	1000
LR Decay scheduler	Constant
Optimizer	AdamW
Optimizer coefs	beta1 = 0.9, beta2 = 0.999

C.2.4. LANGUAGE TRANSLATION MODEL → Enc-Dec

We train an encoder-decoder-based model on WMT-17 with hyperparameters presented in Table 15. The model is inspired by the attention paper (Vaswani et al., 2017). We follow the hyperparameter setting in (Devlin et al., 2019) to train all models. The training phase takes ≈ 8 hours on 32 - Google Cloud TPU v3 cores.

D. Codebase

Our ViT and SWINV2 codebase is made by modifying the TIMM code base of hugging-face vision transformers (Wightman, 2019). We add sparsity layers to various models and modify the training loop to support training recipes presented in this work. Similarly, we modify the jax-based codebases for T5X and Language translation model experiments. The source code is available at GitHub.

Table 15. Model configurations and hyperparameters for training model on WMT.

Number of Encoder Layers	6
Number of Decoder Layer	6
Hidden Dimension Size	1024
Feed-Forward Dimension Size	4096
Number of Attention Heads	16
Max Sequence Length	256
Training Dataset	WMT-17
Testing Dataset	WMT-14
Batch Size	512
Training Steps	200K
Learning Rate	0.0625
LR Warmup Steps	1000
Decay Factor	0.5
Optimizer	Adam
Optimizer coefs	beta1 = 0.9, beta2 = 0.92

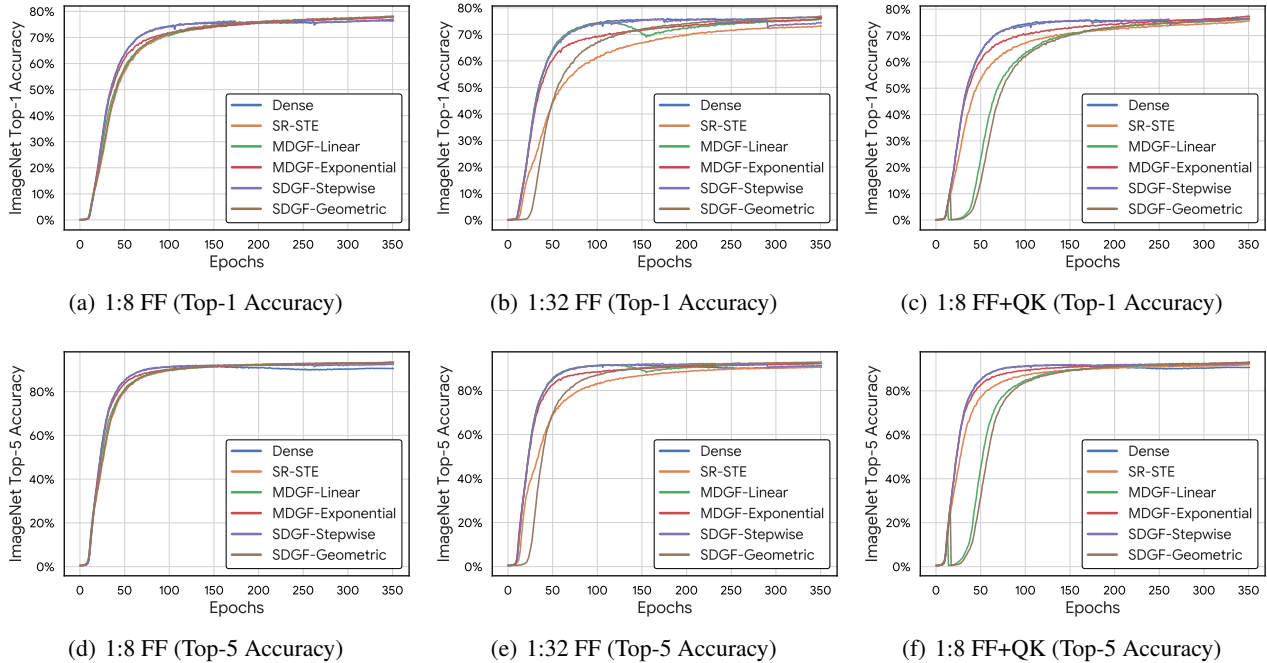


Figure 6. Training Epochs vs Accuracy graph for different sparsity targets. We train ViT-Base on ImageNet-1K.

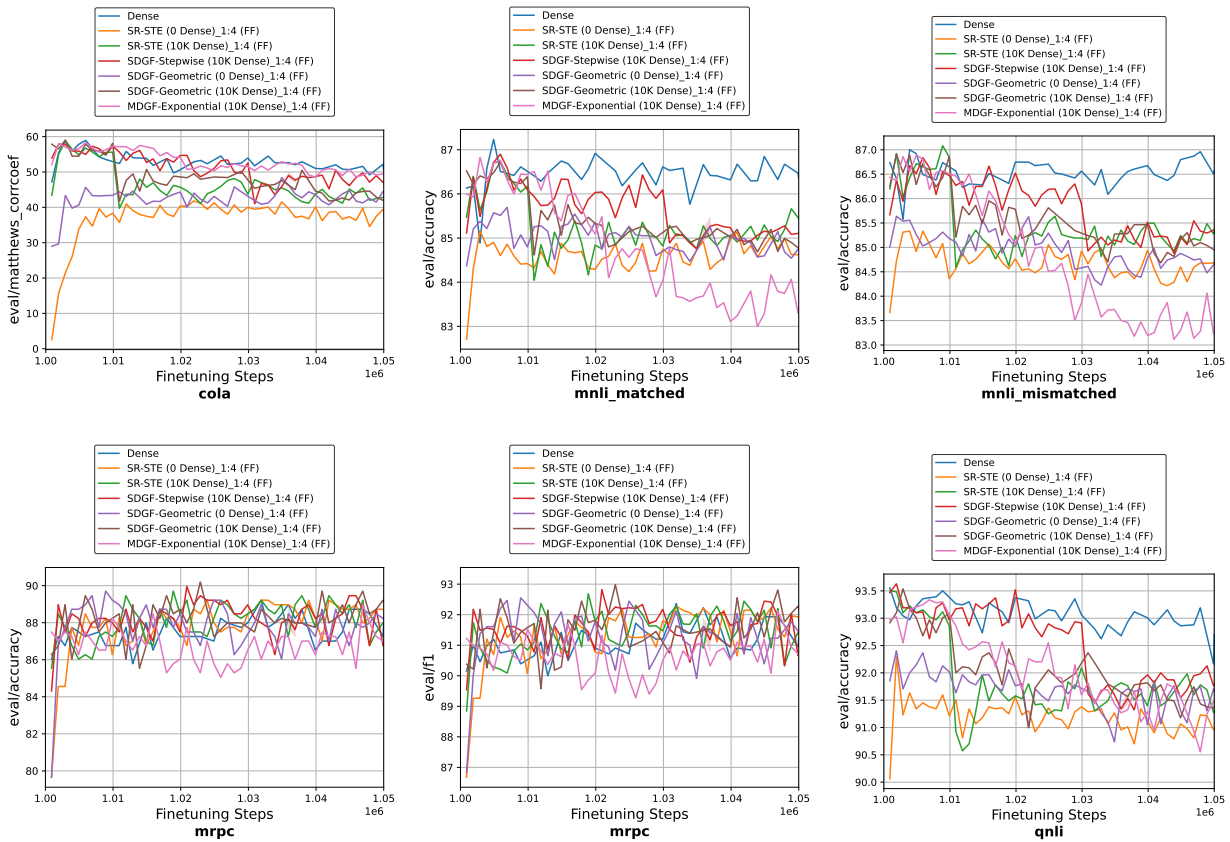


Figure 7. Per-task evaluations for T5X-Base model finetuned on the GLUE dataset for 50 K steps.

E. FLOPS Calculation

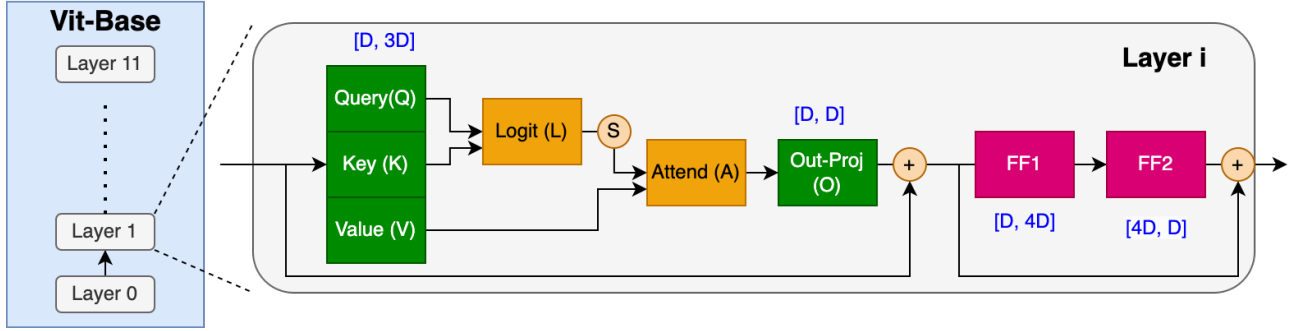


Figure 8. Operations for ViT base model. For sake of brevity, we only include the operators that take significant runtime. Parameter dimensions are mentioned in blue text near the corresponding operators.

Figure 8 shows various operators in ViT base model. The breakdown of flops, Table 16, shows that FF accounts for majority of the FLOPS and thus would be our main avenue of sparsification.

FLOPS (G)	Q/K/V/O	L/A	FF1/FF2
Dense	2.77	0.7	11.1

Table 16. Operator wise FLOPS breakdown for ViT-base.

We calculate the total number of flops for the model as follows.

$$\begin{aligned}
 FLOPS_{tot} &= FLOPS_{SA} + FLOPS_{FF} * S_{FF} \\
 FLOPS_{SA} &= FLOPS_Q + FLOPS_K + FLOPS_V + FLOPS_L + FLOPS_A + FLOPS_O \\
 FLOPS_{FF} &= FLOPS_{FF1} + FLOPS_{FF2}
 \end{aligned}$$

$FLOPS_{SA}$ is number of flops in self-attention layers which consists of QKV generation, 2 einsums (Logit and Attend) and output projection(O).

$FLOPS_{FF}$ is number of flops of the 2 feed-forward layers.

Using these equations, We list the total FLOPS of ViT-base for various sparsity targets in Table 17.

Sparsity : S_{FF}	$FLOPS_{SA}$	$FLOPS_{FF}$	$FLOPS_{tot}$
Dense : 1.0	12.51	22.19	34.71
2:4 (FF) : 0.5	12.51	11.1	23.61
1:4 (FF) : 0.25	12.51	5.55	18.06
1:8 (FF) : 0.125	12.51	2.77	15.29
1:16 (FF) : 0.0625	12.51	1.39	13.90
1:32 (FF) : 0.03125	12.51	0.69	13.20
1:128 (FF) : 0.0078125	12.51	0.17	12.69

Table 17. FLOPS(G) calculation for various level of sparsity in ViT-Base.